small NANO MICRO

Aerosol printing

DOI: 10.1002/smll.200700206

Directed Aerosol Writing of Ordered Silica Nanostructures on Arbitrary Surfaces with Self-Assembling Inks

*Jiebin Pang, John N. Stuecker, Yingbing Jiang, Ajay J. Bhakta, Eric D. Branson, Peng Li, Joseph Cesarano III, David Sutton, Paul Calvert, and C. Jeffrey Brinker**

This paper reports the fabrication of micro- and macropatterns of ordered mesostructured silica on arbitrary flat and curved surfaces using a facile robot-directed aerosol printing process. Starting with a homogenous solution of soluble silica, ethanol, water, and surfactant as a self-assembling ink, a columnated stream of aerosol droplets is directed to the substrate surface. For deposition at room temperature droplet coalescence on the substrates and attendant solvent evaporation result in continuous, highly ordered mesophases. The pattern profiles are varied by changing any number of printing parameters such as material deposition rate, printing speed, and aerosol-head temperature. Increasing the aerosol temperature results in a decrease of the mesostructure ordering, since faster solvent evaporation and enhanced silica condensation at higher temperatures kinetically impede the molecular assembly process. This facile technique provides powerful control of the printed materials at both the nanoscale and microscale through chemical self-assembly and robotic engineering, respectively.

Keywords:
- aerosols
- mesostructures
- micropatterns
- roboprinting
- self-assembly

[*] Dr. J. Pang, A. J. Bhakta, Prof. C. J. Brinker
NSF/UNM Center for Micro-Engineered Materials
Department of Chemical and Nuclear Engineering
The University of New Mexico
Albuquerque, NM 87131 (USA)
Fax: (+1) 505-272-7336
E-mail: cjbrink@sandia.gov

Dr. J. Pang, Dr. J. N. Stuecker, Dr. Y. B. Jiang, E. D. Branson, Dr. J. Cesarano III, Prof. C. J. Brinker
Advanced Materials Lab, Sandia National Laboratories
1001 University Blvd SE
Albuquerque, NM 87106 (USA)

Dr. Peng Li
Transmission Electron Microscopy Labs
The University of New Mexico
Albuquerque, NM 87131 (USA)

Dr. D. Sutton
Imperial Chemical Industries (ICI) Strategic Technology Group
Wilton Center, Wilton, Redcar TS10 4RF (UK)

Prof. P. Calvert
Department of Materials and Textiles
University of Massachusetts Dartmouth
285 Old Westport Road, North Dartmouth, MA 02747 (USA)

1. Introduction

Mesostructured and mesoporous materials have been the subject of great scientific and technological interest since the discovery of the Mobil composition of matter (MCM) family of materials by Mobil researchers.[1–4] These materials have applications in catalysis,[5] separation,[6] nanoreactors,[7] nanofluidics,[8,9] sensing,[10] confined and templated synthesis,[11] bioencapsulation,[12] and low-dielectric- constant insulators.[13] The mostly thoroughly developed mesostructured materials are in the form of powders prepared by hydrothermal synthesis.[1] Powders are useful for catalysis, column fillers, and drug delivery; however, thin films are of particular interest for microelectronics, sensors, and membrane separations. Evaporation-induced self-assembly (EISA) was pioneered by Brinker and colleagues for the synthesis of highly ordered mesoporous silica and mesostructured organic–inorganic nanocomposites via simple dip- or spin-coating procedures.[10,14–19] Relevant to the present study, aerosol-assisted EISA was demonstrated as a means to generate highly ordered micrometer- to nanometer-sized powders.[16,17] Here we report a columnated aerosol-assisted

EISA writing process to print arbitrary patterns of nanostructured materials on arbitrary surfaces. Starting with a homogeneous solution of soluble silica, ethanol, water, and surfactant prepared near a pH value of 2 to minimize the siloxane condensation rate, solvent evaporation accompanying aerosol generation induces silica–surfactant self-assembly into liquid-crystalline mesophases confined within spherical droplets. If the droplets are solidified by complete drying, heating, or exposure to catalyst they can be captured on a filter and maintained as spheres.[16,17] However, fluid liquid-crystalline droplets coalesce when deposited on a surface forming a thin-film mesophase[20] similar to that formed by dip- or spin-coating. Whether the product is a particle or a film depends largely on the extent of drying and siloxane condensation of the droplet prior to its contacting the surface and the relative rates of flow and wetting, coalescence, and solidification on the surface.

For applications in sensors, micro-optoelectronic devices and microelectromechanical systems (MEMS), micropatterning of mesostructured materials is very important.[21] Several microfabrication techniques, such as surface-regulated growth,[19,22,23] lithographic micromolding,[24–29] and optical lithography[18,30] have been reported for micropatterning of mesostructured materials. However, most of these lithographic processes are complicated and require flat substrates (e.g., silicon, silica, and mica).[18,19,21–30] Recently, mesostructured silica micropatterns on polymer substrates have been reported through transferring the prefabricated micropatterns from a silicon substrate to a polymeric substrate;[31] however, it still requires several complicated steps.[31] Developing a facile micropatterning technique that is also friendly to various substrates remains challenging. Mirkin and colleagues patterned organic–inorganic composite nanostructures from sol-based inks by dip-pen nanolithography (DPN),[32] which showed high-resolution features but not periodic mesostructural order. Our group demonstrated micropatterning of mesostructured materials through micropen lithography and ink-jet printing techniques.[19] One problem for micropen lithography to print EISA materials is substantial wetting and spreading (e.g., 1-mm-width lines using a 50-μm-diameter micropen) because the micropen directly deposits and casts the original dilute solution on substrates without any preceding solvent evaporation.[19] Therefore, the freshly printed materials remain fluid, making it difficult to print uniform patterns on curved or nonhorizontal substrates. A commercial ink-jet printer has similar limitations and requires specific substrates.[19] Furthermore, none of the above techniques have been employed to pattern mesostructured silica materials on curved substrates.

Robot-controlled deposition (robocasting) deposits ceramic precursors on arbitrary substrates via extrusion through a syringe.[33–35] Here we extend robocasting to directly write nanostructured silica at micro- and macroscales on arbitrary substrates (e.g., silicon wafers, glass slides, polymeric transparencies, and curved glass surfaces) using an aerosol droplet generator[16,17] mounted on a multiaxis print head (see a schematic illustration in Figure 1a). This hybrid approach comprises three technologies: self-assembling inks,[10,14–19] aerosol-assisted self-assembly,[16,17] and robot-controlled deposition.[33–35] It is of great interest not only in furthering applications of mesostructured materials and nanocomposites but also in developing scientific insights into the EISA process and its extension to directed assembly.

2. Results and Discussion

2.1. Micro- and Macropatterns

Using this printer (Figure 1a), we have successfully printed self-assembled silica–surfactant nanocomposites on various substrates (e.g., silicon wafers, glass slides, polymeric transparencies, and curved glass surfaces). All the results discussed below are based on printed silica–surfactant micro- and macropatterns. Samples were not calcined or extracted, although as we mention later and in the Experimental Section, we can extract the surfactant using the UV/ozone calcination process reported previously.[30,36,37] Patterns were created using computer-aided design software. Figure 2(a–c, e, f) shows photographs of several typical patterns (e.g., straight lines, spiral lines, crossed lines, and films) printed using the three general classes of structure-directing agents (SDAs): the cationic surfactant, cetyltrimethylammonium bromide (CTAB; Figure 2a–c),the nonionic surfactant, Brij-56 (B56; Figure 2e), and the block copolymer, Pluronic 123 (P123; Figure 2f). For all SDAs, the lines and films are continuous and uniform, demonstrating the generality of the technique. Deposition and pH conditions are designed to minimize the siloxane rate and

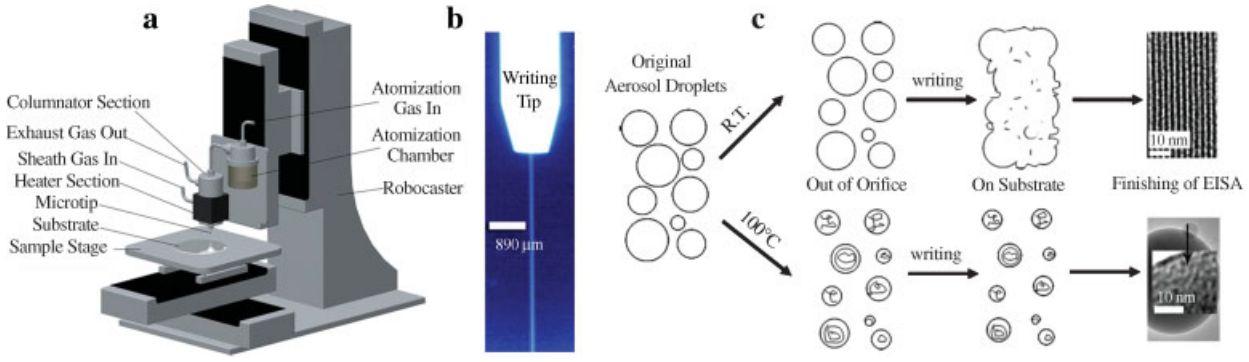

Figure 1. a) Schematic illustration of the aerosol-droplet generator mounted on the robocaster, b) photograph of the aerosol stream, and c) proposed mechanism of EISA during the writing process.

small NANO MICRO

therefore maintain the fluidity of the drops. This allows the deposited aerosol particles to coalesce and self-assemble into continuous lines or a continuous film on the substrate (see a proposed mechanism in Figure 1c). The films were printed by increasing the density of lines in a specific area so that the wet lines slightly overlap, coalescing into a continuous film. These films facilitate the characterization of the mesostructures, using, for example, X-ray diffraction (XRD) measurements. As seen in Figure 2d, a continuous intersection is formed even at the crossing site of printed lines. A representative scanning electron microscopy (SEM) image of the printed lines is shown in Figure 2h, showing that the surface is smooth and the material is continuous with no apparent evidence of the original spherical nature of the deposited drops.

Robot-controlled printing using self-assembling inks enables conformal printing of mesostructured silica on surfaces of arbitrary shape. Figure 2i shows a photograph of a mesostructured silica line printed on a curved glass vial surface using P123 as the SDA. The printed lines show the same uniformity as those printed on flat substrates. Using a shutter allows discontinuous printing. In this way, we can fabricate more complex patterns of mesostructured silica by turning the shutter on and off to block and unblock the printing stream. Figure 2j shows a typical printed pattern that contains 1 mm of short silica lines with a spacing of 2 mm.

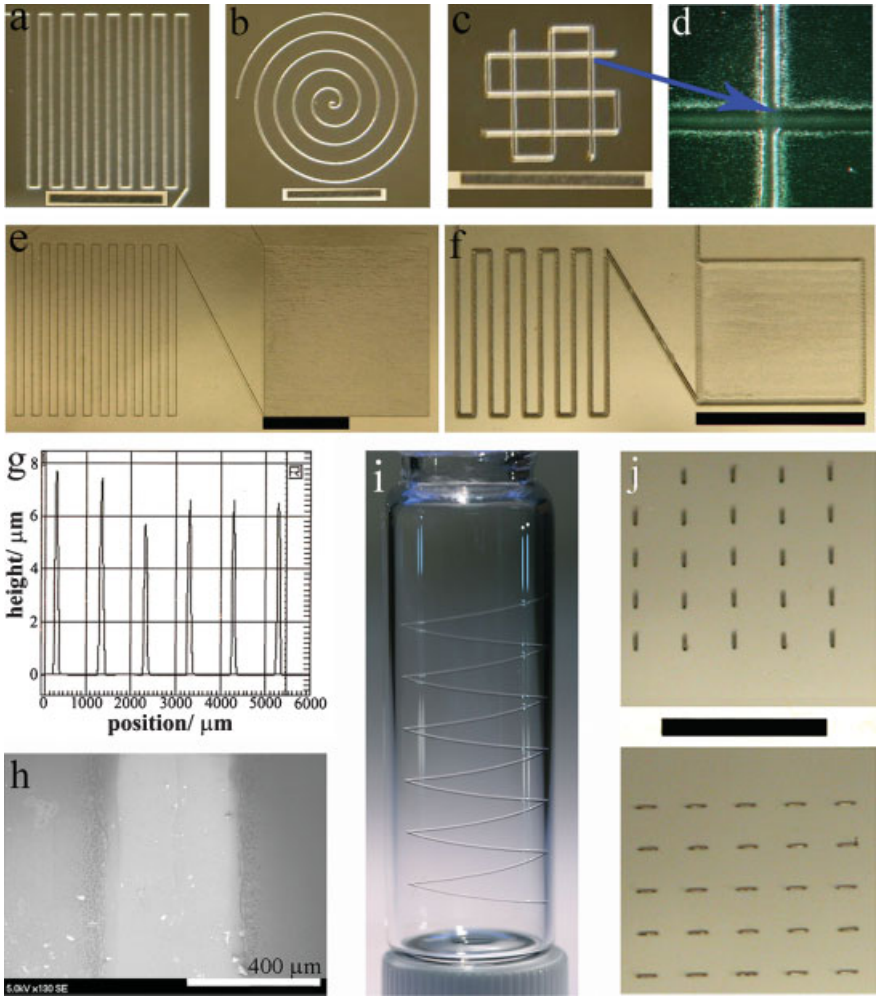

Figure 2. Photographs of mesostructured silica patterns printed by the aerosol robocaster at 10 mm s^{-1} and at RT using a–c) CTAB, e) B56, and f,i,j) P123 as structure-directing agents. d) An enlarged optical microscopy image of one intersection of the patterns in image (c). g) Contact profilometry scan of the printed lines in image (a). h) A representative SEM image of the printed lines in image (f). i) 3D spiral. j) Discontinuous pattern of lines. Photograph scale bars: 10 mm.

The contact profilometry scan confirmed that the printed micrometer-sized lines are reasonably uniform. For example, the printed CTAB-directed mesostructured silica lines are about 7 μm in height and 130 μm in width, and the spacing between adjacent lines is about 870 μm (Figure 2g) and quite uniform. Although very thin films are desirable for applications such as separation, continuous self-assembled mesostructured silica films with a thickness of several micrometers are very interesting in MEMS applications.[21] Height and width of the printed lines are easily controlled by the printing speed/substrate velocity and material deposition rate. Figure 3 shows the relationships between the average height and width with printing speed at a constant deposition rate. The height and width decrease with increasing printing speed because of a lower flux of aerosol particles per unit area when the printing speed increases. Although this printing process has not yet reached submicrometer resolution, this facile technique complements the reported

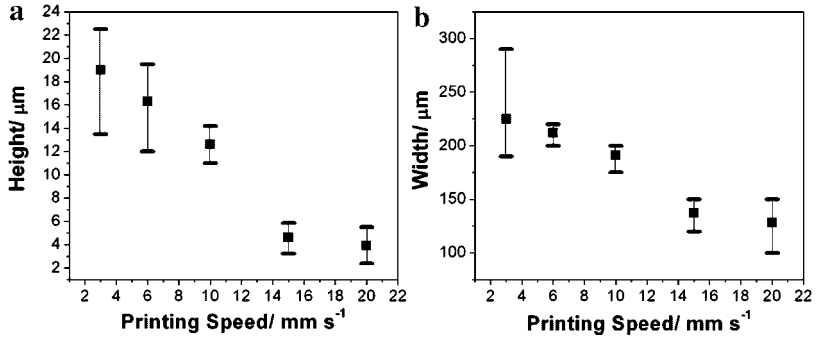

Figure 3. Height (a) and width (b) of the P123-templated silica lines printed at RT as a function of printing speed.

micropatterning techniques.[18,19,22–32] Additionally, because the droplet size distribution is centered at a 7-μm diameter (see Supporting Information Figure S2) is « the line width, further stages of columnation should enable micrometer-sized line widths to be obtained.

2.2. Ordered Mesostructures

The mesostructure of the printed materials was evaluated by XRD and transmission electron microscopy (TEM) of the printed patterns and films. All printed silica–surfactant nanocomposites exhibit highly ordered mesostructures. Figure 4 shows the XRD patterns of the materials printed from CTAB, B56, and P123 containing systems. All of the samples exhibit intense XRD patterns at low angle, similar to those reported for the mesostructured films,[20,31] indicating that highly ordered mesostructures are formed. For example, the CTAB-templated silica nanocomposite exhibits highly intense reflections at 3.5 and 1.77 nm (Figure 4a), which are indexed as the (100) and (200) planes of a two-dimensional (2D) hexagonal mesostructure.[29] TEM images (Figure 9a) of the CTAB-templated silica show a ≈3.5-nm spacing of bright lines and a ≈4.0-nm center-to-center spacing of bright dots, which is consistent with the XRD results (Figure 4a). The absence of (110) and (210) diffraction peaks, which are typical for powders, indicates the hexagonal mesophase is oriented parallel to the substrate as observed generally for films.[20,31] The printed lines exhibit diffraction patterns similar to films (Figure 4b) but with less diffraction due to the lower amount of printed material. The lines printed on glass slides and polymeric transparencies also exhibit highly ordered mesostructures (see Supporting Information Figure S1). The printed materials with B56 as SDA show a diffraction peak at 4.4 nm (Figure 4c), which is indexed as (100) for a hexagonal mesostructure with a lattice constant (a) of 5.1 nm. Figure 5 (a, b) shows the TEM images of the B56-templated nanocomposite, which is consistent with a 2D hexagonal mesostructure. As measured from the image, the distance between the bright lines is about 4.4 nm (Figure 5a) and the center-to-center distance of the bright dots is about 5.2 nm (Figure 5b), which agree well with the XRD results (Figure 4c). Lamellar or 2D hexagonal mesophases are obtained for the P123-templated films. Figure 4d shows strong 200, 300, and 400 reflections for a lamellar film.

CTAB-templated, 2D hexagonal mesophase films formed by EISA using dip- or spin-coating show orientation of the cylindrical channel axes parallel to the substrate surface but

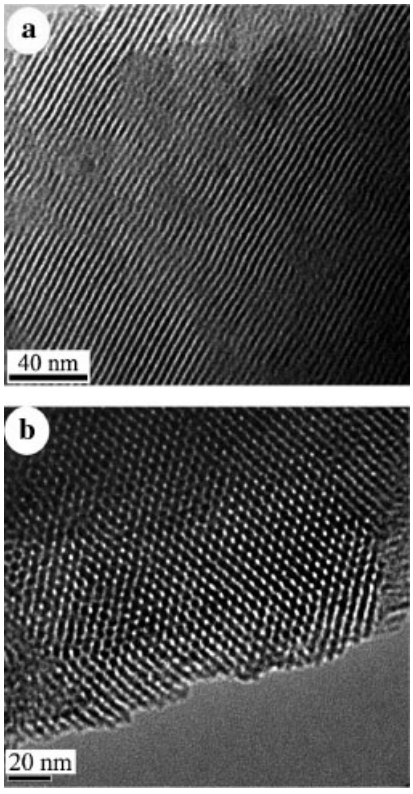

Figure 5. Representative TEM images taken perpendicular to (a) and parallel to (b) the cylinder axis direction for a 2D hexagonal mesophase line printed at 10 mm s^{-1} and RT using B56 as a template. The TEM samples were directly scratched from the materials.

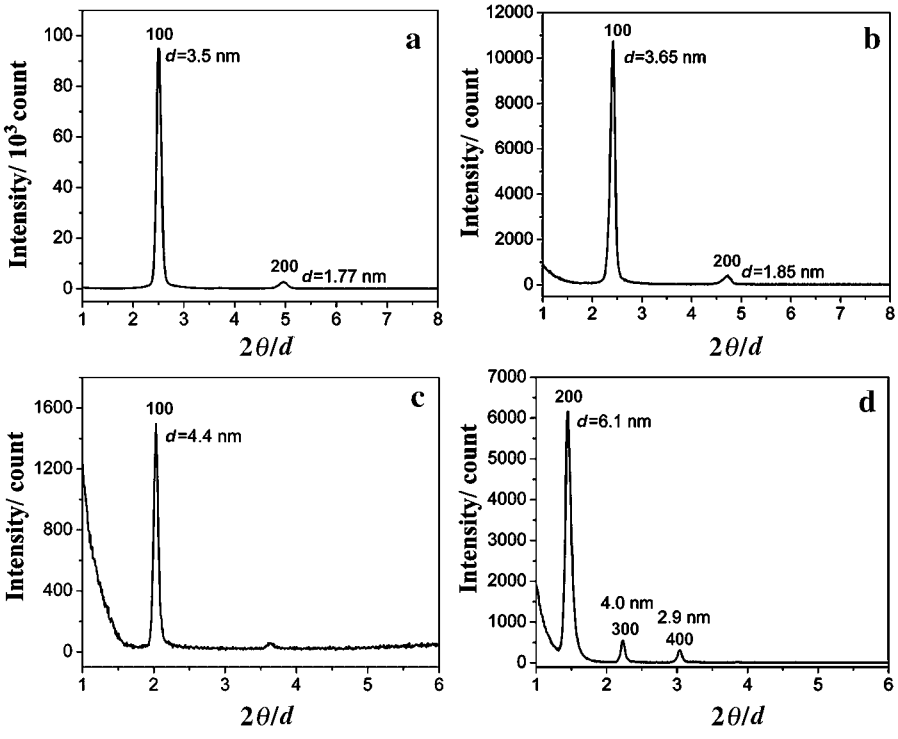

Figure 4. XRD patterns for the films (a,c,d) and lines (b) printed on a Si wafer at 10 mm s^{-1} and RT using a,b) CTAB, c) B56, and d) P123 as templates.

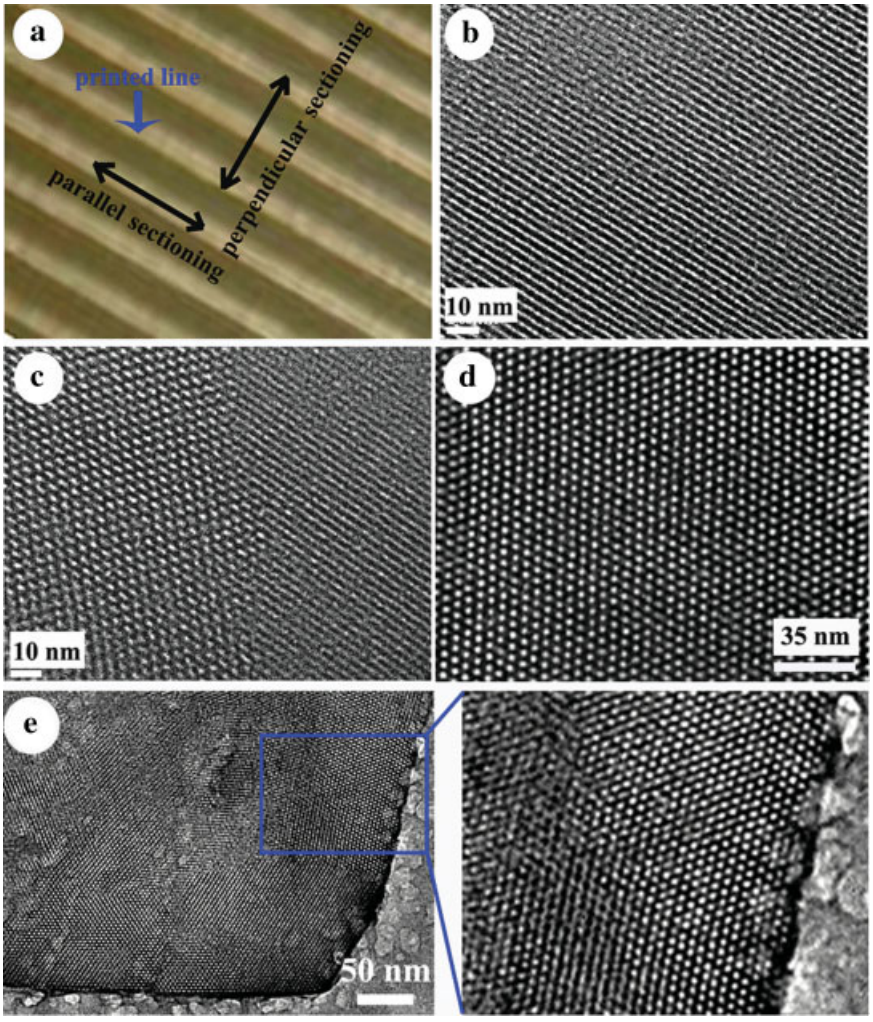

Figure 6. Representative cross-section TEM images taken from the cross sections parallel to (b,c) and perpendicular to (d,e) the printing direction of a silica/CTAB line (a).

there is no in-plane orientation.[14] As the roboprinting process imposes shear on the depositing drops and confines the printed line within the rather narrow liquid–vapor boundaries ($\approx 10 \times 150\ \mu m^2$) of the printed line, we questioned whether the mesophase shows any orientation with respect to the line-printing direction. Figure 6a shows an optical image of a CTAB/silica line sample and defines the line sectioning parallel to and microtoming perpendicular to the printing direction. The parallel section shows stripes oriented parallel to the line direction, as expected (Figure 6b), with very few hexagonally oriented regions (Figure 6c) resulting from mesophase oriented normal to the printing direction. The microtomed cross section (Figure 6d and Figure S3 in Supporting Information) shows rather large domains of hexagonally arranged dots corresponding to cylindrical mesophases aligned parallel to the writing direction. Surface-confined regions especially show this parallel alignment (Figure 6e). This suggests that further confinement of line width and height (attainable with newer, more columnated printing heads) will further enhance alignment. Moreover, the effect of substrate on the self-assembled mesostructure is under investigation in our lab, for example, directed-writing nanostructures on a prepatterned or pretreated substrate surface.

2.3. Temperature Effect

EISA within an aerosol droplet is sensitive to temperature because an increase in temperature increases both the rates of drying and siloxane condensation.[20] We have printed different CTAB-templated silica materials while changing the temperature of the heater section (Figure 1a) located upstream of the printhead. Figure 7 shows photographs and SEM images of the films and lines printed at room temperature (RT), 50, 80, and 100 °C. As seen from Figure 7, the films change from transparent (RT, 50 °C) to translucent (80 °C) to opaque (100 °C). At 50 °C and below, the extent of silica condensation is initially very low and the aerosol droplets remain fluid enough to coalesce into a continuous phase resulting in a smooth surface (see a proposed mechanism in Figure 1c, and SEM images in Figure 7). The observed line width is about 130–140 μm, consistent with the profilometry measurement (Figure 2g). However, when the temperature increases further (e.g., 80 °C), the aerosol droplets contact the substrate at a more advanced stage of drying and the film begins to acquire a particlelike quality (more satellites are observed in SEM, Figure 7) and brittleness, which leads to cracking. When the temperature increases to 100 °C, the aerosol droplets are dry or almost dry before reaching the substrate; therefore, an opaque film composed of dry spherical particles with sizes ranging from 1 to 7 μm is formed (see a proposed mechanism in Figure 1 and SEM images in Figure 7, and a statistic analysis of particle size distribution in Figure S2). The samples printed at 100 °C easily peeled off the substrate due to the loose nature of the particle aggregates. Similar SEM images were obtained for the printed films (Figure S2).

The competition between self-assembly and evaporation is also evident at the nanoscale. Figure 8 shows the XRD patterns of the samples printed at different temperatures and Figure 9 shows the corresponding TEM images. The film prepared at RT shows highly intense reflections, indicating a highly ordered mesostructure (see the TEM images in Figure 9a); however, the samples printed at 50 and 80 °C show single-peak patterns (inset of Figure 8) with much lower intensity, consistent with their partially ordered wormlike mesostructures, as evident in TEM (Figure 9b, c). Small regions of the sample show mesoscale ordering (inset of Figure 9c). The sample printed at 100 °C does not show any X-ray diffraction, indicating a nonordered structure. TEM

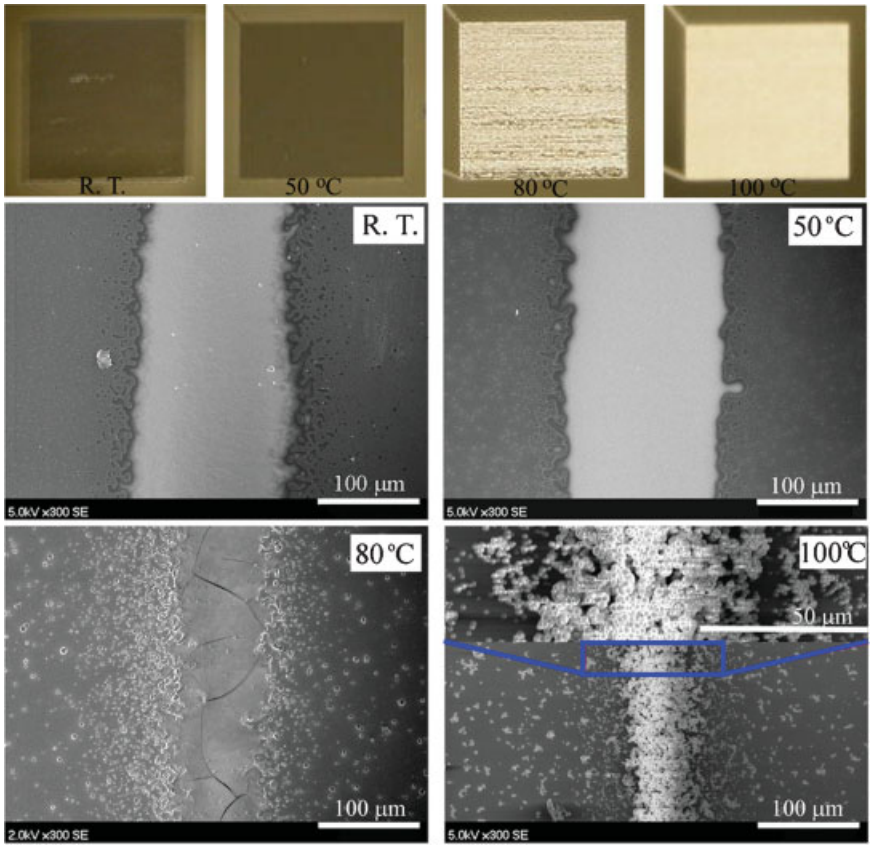

Figure 7. Photographs (top) and SEM images (middle and bottom) of the CTAB-templated materials printed at 10 mm s^{-1} and different temperatures.

images (Figure 9d) of this sample show spherical particles with a disordered mesostructure.

These results emphasize the competition between coalescence and self-assembly, driven by interfacial energy and noncovalent interactions, and solidification due to thermally promoted evaporation and siloxane condensation. As we reported previously, heating causes EISA and solidification of individual particles allowing their collection as nanostructured powders.[16,17,20] Depending on the residence times at different temperatures and different atmospheres the outcome of this competition varies. For example, the significant solvent evaporation in the drying zone of the reactor we used for particle formation (a residence time of ≈3 s[16] at 50 °C) allowed evaporation and self-assembly to occur before thermally promoted solidification. During printing, however, less solvent evaporation of the aerosol droplets occurs before the heater section due to a shorter residence time (≈0.5 s) and a smaller-diameter (4 mm) tube, which is saturated with solvent/N_2. This causes self-assembly to be kinetically impeded by the suddenly faster solvent evaporation and enhanced silica condensation at higher temperatures when printing above RT, although the residence time (≈0.067 s) of the aerosol droplets in the heater section is much shorter. The proposed mechanism in Figure 1c is based on the experimental results and is also supported by our previous work.[16,17,20]

Although the above results are based on mesostructured silica–surfactant nanocomposites, surfactants have been successfully removed by UV/ozone photocalcination,[30,36,37] resulting in mesoporous materials. Fourier transform infrared (FTIR) and XRD results demonstrate the removal of surfactant and maintenance of ordered structures. For example, as seen from the FTIR results (Figure S4), the C–H stretching bands at 2930 and 2852 cm^{-1} and the C–H deformation band at 1945 cm^{-1} of the surfactant molecules in the printed CTAB-silica nanocomposites practically vanish after 3 h of photocalcination.[36,37] Importantly, the CTAB-templated materials after photocalcination show similar diffraction patterns (Figure S5) with slightly decreased intensity compared to the uncalcined samples.

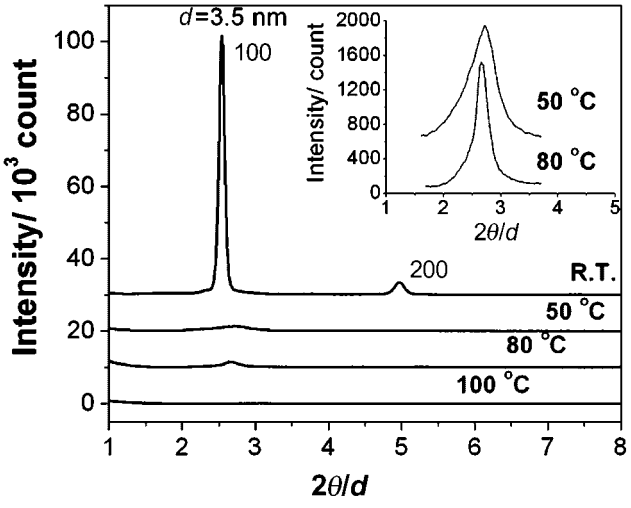

Figure 8. XRD patterns of the CTAB-templated materials printed at 10 mm s^{-1} and different temperatures on Si wafers.

3. Conclusions

Highly ordered mesostructured silica patterns have been printed on various substrates, such as silicon wafers, glass slides, polymeric transparencies, and curved glass surfaces, by a facile printing technique using an aerosol-droplet generator mounted to a multiaxis robocaster. The aerosol droplets containing silica, surfactant, and solvent are deposited on a substrate in a fluid stage, allowing coalescence into a continuous phase. During the whole evaporation process molecular self-assembly continues to proceed, forming a highly ordered mesostructure. The height and width of printed lines decrease with increasing printing speed. The highly

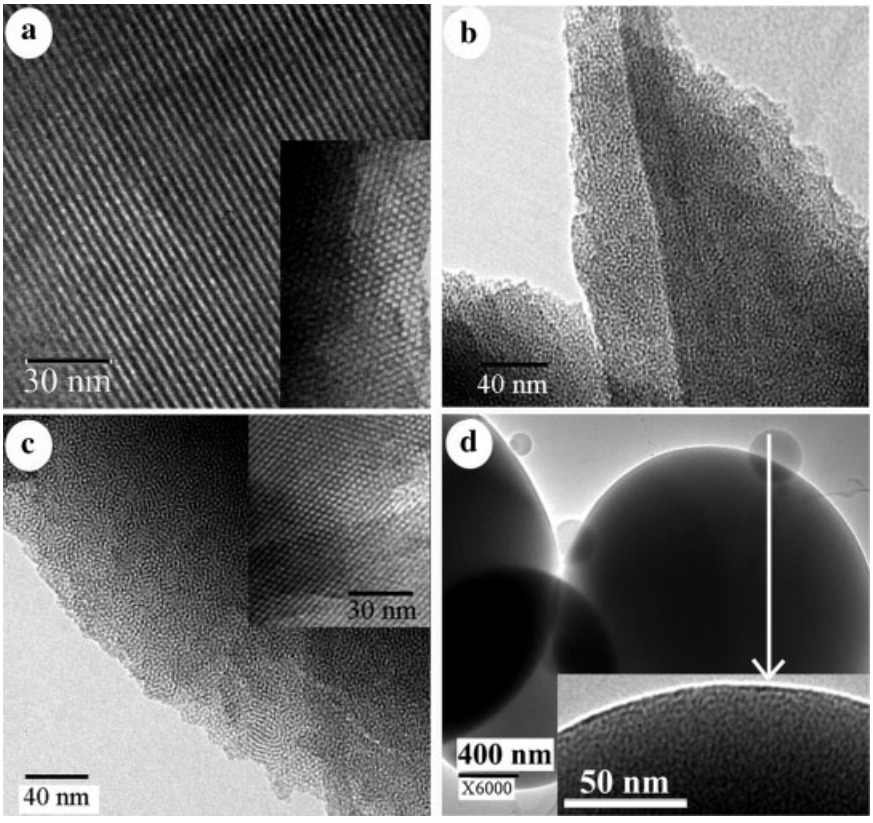

Figure 9. Representative TEM images for the nanocomposites printed at 10 mm s^{-1} and a) RT, b) 50 °C, c) 80 °C, and d) 100 °C using CTAB as a template. The TEM samples were directly scratched from the materials.

ordered mesostructures are characterized by XRD and TEM. Increasing the aerosol temperature results in a decrease of the mesostructure ordering due to the faster solvent evaporation and silica condensation at higher temperatures. The surfactant molecules can be successfully removed by photocalcination of the silica–surfactant nanocomposites. Use of this technique to fabricate functional self-assembled nanostructures is underway in our lab.

4. Experimental Section

Precursor preparation: In a typical preparation of the self-assembling ink from CTAB, CTAB, (Aldrich, 1.2 g) was dissolved in a mixture of ethanol (26.7 g) and aqueous HCl (0.05 mol L^{-1}, 2.5 mL). Tetraethylorthosilicate (TEOS, 6.5 mL) was then added into the solution under stirring. After 2 h of stirring, the sol precursor was ready for printing or was stored in a refrigerator for printing within 2 days. In a typical preparation of the self-assembling ink from P123: Pluronic P123 (P123, $(EO)_{20}(PO)_{70}(EO)_{20}$, BASF product, 2.0 g), a triblock copolymer of poly(ethylene oxide) (PEO) and poly(propylene oxide) (PPO) was dissolved in a mixture of ethanol (20 g), H_2O (1.2 g) and aqueous HCl (1 mol L^{-1}, 0.8 g). After the surfactant was completely dissolved, TEOS (4.5 mL) was added into the solution under stirring. After continuous stirring for 2 h, the sol precursor was ready for printing or was stored in a refrigerator for printing within 2 days. In a typical preparation of the self-assembling ink from B56, nonionic surfactant Brij-56 (B56, $C_{16}EO_{10}$, Aldrich, 1.6 g) was dissolved in a mixture of ethanol (24 g) and aqueous HCl (0.07 mol L^{-1}, 2.5 mL). TEOS (6 mL) was then added into the solution under stirring. After continuous stirring for 2 h, the sol precursor was ready for printing or was stored in a refrigerator for printing within 2 days.

Printing method: The gas flows (e.g., atomization gas, sheath gas, and exhaust gas) were controlled by an Optomec M^3D aerosol-droplet generator system (Optomec Inc, Albuquerque, NM). Atomization of the sol precursor is induced in the atomization chamber through a venturi. The small droplets are entrained in an atomization gas (N_2) through the columnator section where the particle stream is narrowed. The stream is then directed through a microtip with an orifice of 250 μm and with the aid of a sheath gas (N_2). The aerosol temperature was controlled by the heater section (Figure 1a) located before the tip, whereas the substrates were maintained at RT for all the printing experiments. Both the design of patterns and the printing process (e.g., *x*–*y*–*z*– rotational movements) were controlled by a custom software package developed specifically for the robocaster. The distance between the tip and the substrate was kept at 5 mm and controlled by *z* movement. The printing was performed by control of the *x* and *y* movements of the sample stage. An additional step was needed to control a fourth motor and fixture that held the glass vial, allowing printing of the materials on the outer curved surface of the vial. Fresh and clean substrates were used as received without any further cleaning. One advantage of this robotically controlled technique is the conformal deposition of self-assembled materials on various, even nonflat substrates, of interest. We selected silicon wafers, glass slides, polymeric transparencies, and glass vials as substrates for investigation and demonstration.

Characterization: TEM images were taken using a JEOL 2010 microscope operated at 200 kV. XRD patterns were recorded on a PANalytical X'Pert PRO X-ray diffractometer operating at 45 kV, 40 mA (CuKα radiation, $\lambda = 0.15406$ nm). Contact profilometry measurement was performed on a Dektak3 Surface Profile Measuring System. SEM images were taken using a Hitachi S-5200 electron microscope operating at an acceleration voltage of 5.0 kV. Photocalcination of the silica–surfactant nanocomposites was performed by exposure of the substrate-supported materials to UV light ($\lambda = 184$–257 nm) produced by a low-pressure Hg discharge grid lamp in an uncoated quartz envelope, maintained in a closed chamber under ambient laboratory conditions. FTIR spectra of the materials scratched from the substrates were measured in the form of KBr powder-pressed pellets on a Bruker Vector 22 FT-IR spectrometer.

Acknowledgements

This work was financially supported by the ICI Company (J.P.), DOE Office of Basic Energy Sciences (C.J.B.), Army Research Office (C.J.B.), and Air Force Office of Scientific Research (C.J.B.). Sandia is a multiprogram laboratory operated by Sandia Corporation, a Lockheed Martin Company, for the United States Department of Energy's National Nuclear Security Administration under Contract DE-AC04-94AL85000. We thank Mr. A. Cook for the assistance on the contact profilometry measurement.

[1] C. T. Kresge, M. E. Leonowicz, W. J. Roth, J. C. Vartuli, J. S. Beck, *Nature* **1992**, *359*, 710.
[2] F. Schüth, W. Schmidt, *Adv. Mater.* **2002**, *14*, 629.
[3] A. Stein, *Adv. Mater.* **2003**, *15*, 763.
[4] M. E. Davis, *Nature* **2002**, *417*, 813.
[5] A. Corma, H. Garcia, *Adv. Synth. Catal.* **2006**, *348*, 1391.
[6] G. Xomeritakis, C. M. Braunbarth, B. Smarsly, N. Liu, R. Kohn, Z. Klipowicz, C. J. Brinker, *Microporous Mesoporous Mater.* **2003**, *66*, 91.
[7] C. G. Wu, T. Bein, *Science* **1994**, *264*, 1757.
[8] D. Stein, M. Kruithof, C. Dekker, *Phys. Rev. Lett.* **2004**, *93*, 035901.
[9] H. Daiguji, P. D. Yang, A. Majumdar, *Nano Lett.* **2004**, *4*, 137.
[10] Y. F. Lu, Y. Yang, A. Sellinger, M. C. Lu, J. M. Huang, H. Y. Fan, R. Haddad, G. López, A. R. Burns, D. Y. Sasaki, J. Shelnutt, C. J. Brinker, *Nature* **2001**, *410*, 913.
[11] J. L. Shi, Z. L. Hua, L. X. Zhang, *J. Mater. Chem.* **2004**, *14*, 795.
[12] M. Hartmann, *Chem. Mater.* **2005**, *17*, 4577.
[13] R. A. Pai, R. Humayun, M. T. Schulberg, A. Sengupta, J. N. Sun, J. J. Watkins, *Science* **2004**, *303*, 507.
[14] Y. F. Lu, R. Ganguli, C. A. Drewien, M. T. Anderson, C. J. Brinker, W. L. Gong, Y. X. Guo, H. Soyez, B. Dunn, M. H. Huang, J. I. Zink, *Nature* **1997**, *389*, 364.
[15] A. Sellinger, P. M. Weiss, A. Nguyen, Y. F. Lu, R. A. Assink, W. L. Gong, C. J. Brinker, *Nature* **1998**, *394*, 256.
[16] Y. F. Lu, H. Y. Fan, A. Stump, T. L. Ward, T. Rieker, C. J. Brinker, *Nature* **1999**, *398*, 223.
[17] a) C. J. Brinker, Y. F. Lu, A. Sellinger, H. Y. Fan, *Adv. Mater.* **1999**, *11*, 579; b) C. J. Brinker, *MRS Bull.* **2004**, *29*, 631.
[18] D. A. Doshi, N. K. Huesing, M. C. Lu, H. Y. Fan, Y. F. Lu, K. Simmons-Potter, B. G. Potter, A. J. Hurd, C. J. Brinker, *Science* **2000**, *290*, 107.
[19] H. Y. Fan, Y. F. Lu, A. Stump, S. T. Reed, T. Baer, R. Schunk, V. Perez-Luna, G. P. López, C. J. Brinker, *Nature* **2000**, *405*, 56.
[20] Y. F. Lu, B. F. McCaughey, D. H. Wang, J. E. Hampsey, N. Doke, Z. Z. Yang, C. J. Brinker, *Adv. Mater.* **2003**, *15*, 1733.
[21] H. K. Jeong, R. Chandrasekharan, K. L. Chu, M. A. Shannon, R. I. Masel, *Ind. Eng. Chem. Res.* **2005**, *44*, 8933.
[22] A. Hozumi, H. Sugimura, K. Hiraku, T. Kameyama, O. Takai, *Nano Lett.* **2001**, *1*, 395.
[23] H. Sugimura, A. Hozumi, T. Kameyama, O. Takai, *Adv. Mater.* **2001**, *13*, 667.
[24] P. Yang, T. Deng, D. Zhao, P. Feng, D. Pine, B. F. Chmelka, G. M. Whitesides, G. D. Stucky, *Science* **1998**, *282*, 2244.
[25] P. Yang, G. Wirnsberger, H. C. Huang, S. R. Cordero, M. D. McGehee, B. Scotto, T. Deng, G. M. Whitesides, B. F. Chmelka, S. K. Buratto, G. D. Stucky, *Science* **2000**, *287*, 465.
[26] P. Yang, A. H. Rizvi, B. Messer, B. F. Chmelka, G. M. Whitesides, G. D. Stucky, *Adv. Mater.* **2001**, *13*, 427.
[27] B. J. Scott, G. Wirnsberger, M. D. McGehee, B. F. Chmelka, G. D. Stucky, *Adv. Mater.* **2001**, *13*, 1231.
[28] G. Wirnsberger, P. Yang, H. C. Huang, B. Scott, T. Deng, G. M. Whitesides, B. F. Chmelka, G. D. Stucky, *J. Phys. Chem. B* **2001**, *105*, 6307.
[29] C. W. Wu, T. Aoki, M. Kuwabara, *Nanotechnology* **2004**, *15*, 1886.
[30] A. M. Dattelbaum, M. L. Amweg, L. E. Ecke, C. K. Yee, A. P. Shreve, A. N. Parikh, *Nano Lett.* **2003**, *3*, 719.
[31] A. Hozumi, T. Kizuki, M. Inagaki, N. Shirahata, *J. Vac. Sci. Technol. A* **2006**, *24*, 1494.
[32] M. Su, X. G. Liu, S. Y. Li, V. P. Dravid, C. A. Mirkin, *J. Am. Chem. Soc.* **2002**, *124*, 1560.
[33] J. E. Smay, G. M. Gratson, R. F. Shepherd, J. Cesarano, J. A. Lewis, *Adv. Mater.* **2002**, *14*, 1279.
[34] J. Cesarano, P. D. Calvert, USA Patent #6027326.
[35] J. N. Stuecker, J. E. Miller, R. E. Ferrizz, J. E. Mudd, J. Cesarano, *Ind. Eng. Chem. Res.* **2004**, *43*, 51.
[36] T. Clark, J. D. Ruiz, H. Y. Fan, C. J. Brinker, B. I. Swanson, A. N. Parikh, *Chem. Mater.* **2000**, *12*, 3879.
[37] a) A. Hozumi, Y. Yokogawa, T. Kameyama, K. Hiraku, H. Sugimura, O. Takai, M. Okido, *Adv. Mater.* **2000**, *12*, 985; b) A. Hozumi, H. Sugimura, K. Hiraku, T. Kameyama, O. Takai, *Chem. Mater.* **2000**, *12*, 3842.

Received: March 21, 2007
Revised: January 13, 2008

